nature climate change

Supplementary information

https://doi.org/10.1038/s41558-024-02108-w

Elevated urban energy risks due to climate-driven biophysical feedbacks

In the format provided by the authors and unedited

Nature Climate Change

Supplementary Information for

Elevated urban energy risks due to climate-driven biophysical feedbacks

Xinchang "Cathy" Li[1], Lei Zhao[1,2,3*], Yue Qin[4,5*], Keith Oleson[6], Yiwen Zhang[1]

[1]Department of Civil and Environmental Engineering, University of Illinois Urbana-Champaign, Urbana, Illinois, USA.

[2]National Center for Supercomputing Applications, University of Illinois Urbana-Champaign, Urbana, Illinois, USA.

[3]Institute for Sustainability, Energy, and Environment (iSEE), University of Illinois Urbana-Champaign, Urbana, Illinois, USA.

[4]College of Environmental Sciences and Engineering, Peking University, Beijing, 100871, China.

[5]Institute of Carbon Neutrality, Peking University, Beijing, 100871, China

[6]Climate and Global Dynamics Laboratory, NSF National Center for Atmospheric Research, Boulder, Colorado, USA.

*emails: leizhao@illinois.edu; qinyue@pku.edu.cn

Contents of this file:

Supplementary Notes 1 | Limitations of the current study

We note two main limitations of this study. First, the effects of urban climate-H&C biophysical feedbacks revealed by this study are likely a dampened signal because of our monthly-based analysis. We use monthly data to build the emulators because of the sparse availability of the required daily data in CMIP6 archive. Evidence exists in the literature that the nonlinear behavior could be more substantial in certain hours of day[1–3] and certain regions of a city[4]. This means an amplified peak energy demand during heat wave events[5] and future higher emission scenarios[6], further increasing the risk for energy infrastructure. Second, the biophysical feedbacks modeled in this study are likely conservative for regions with humid summers. The effect of humidity is captured in the urban canyon of the CLMU, but cooling energy demand for the dehumidification of indoor air is not captured. Studies considering the one-way climate to energy effect suggest the humidity effect is more pronounced at the building level[7] and becomes less so at neighborhood or larger scales[8]. Including humidity in statistical models for electricity demand projections could add an additional 10% increase to electricity demand in the southeastern United States by the end of the century[9]. These results will likely be different if future two-way interactions between climate and energy are considered, as the anthropogenic heat from the additional energy consumption for dehumidification will strengthen the positive feedback loop.

Supplementary Notes 2 | Non-climatic drivers of biophysical feedbacks

Despite the importance of climate-induced biophysical feedbacks in affecting urban H&C energy demand, it has been largely ignored in existing literature, especially at the global scale. Thereby, this study aims to investigate the climate-driven effects alone on urban H&C energy demand by fixing urbanization, H&C ownership rates, and building technology as well as human behavior at present day. Previous studies have evaluated the socioeconomic impacts on future H&C energy use using statistical models, econometric analysis, or Integrated Assessment Models, yet without accounting for the biophysical feedbacks[10–14]. Consequently, prior studies failed to capture the full climate-driven impacts on future energy demand, and tend to largely underestimate the changes and uncertainty in future H&C energy demand under climate change. We find, even without accounting for potential socioeconomic changes, climate-driven biophysical feedbacks alone can lead to 220% (47%) increases (decreases) in future cooling (heating) energy demand under the very high emission scenario. We discuss below the non-climatic drivers to the biophysical feedbacks and their potential implications to future H&C projections: namely, socioeconomic development and our mitigation and adaptation to climate change.

Expected economic and urban growths are likely to further amplify cooling energy demand driven by climate alone. In our results, higher urban density levels can lead to additional cooling demand increase (Supplementary Fig. 2), which agrees with findings from recent studies[10,15,16] and could increase the urban energy burden in cities expecting urban densification. Climate-driven increase in cooling energy demand from this study is also comparable in magnitude with purely socioeconomic-driven increase for residential cooling energy demand as presented in ref.[17] (Supplementary Fig. 3). As both socioeconomic and climate factors are subject to

alteration/amplification by the interactive urban climate-energy biophysical feedbacks we demonstrated in this study, the combined effects would require dynamic simulations with both factors explicitly parameterized to capture the amplification of cooling energy demand caused by the interaction between these factors. We nonetheless provide a simple sum of climate-driven and socioeconomic-driven increases (Supplementary Fig. 3c) to illustrate a lower bound of the combined effects and to add to the context of our results. Dynamic modeling with both changing climate and socioeconomic conditions is needed to reveal the interactions between the socioeconomic and climate effects, which would likely result in much larger magnitude of changes than currently shown as the first-order approximation, especially in the Global South.

That said, human adaptation strategies such as improvements in building insulation, human acclimatization, and wide deployment and utilization of efficient or passive cooling technologies could modify the biophysical feedbacks and partially counteract the projected cooling demand increase. City-wide climate mitigation and adaptation strategies such as white roofs and solar roofs have been shown to reduce cooling energy demand by a few to a few tens of percent in local-scale studies[18–20]. Natural ventilation induces small cooling and heating penalties globally as approximated by CESM2, but generates cooling benefit in places during Spring when it is not too hot (see Supplementary Notes 5 and Supplementary Figs. 4 – 6). The CLMU parameterizes anthropogenic heat release as sensible heat, consistent with most regional scale modeling studies[1]. Alternative cooling technologies that release part of the anthropogenic heat as latent heat (such as using cooling towers) have been shown to significantly reduce anthropogenic heat-induced air temperature increase[21], therefore mitigating the feedback effect and potentially reducing cooling energy demand. For winter heating demand, the feedback effects examined in

this study are consistent with using boiler/furnace heaters rather than heat pumps[22]. Electrification of winter heating (e.g., replacing gas furnaces with heat pumps) would also modify the projected heating demand decrease because of higher efficiencies of heat pumps[23] and the utilization of outdoor heat for indoor heating.

Supplementary Notes 3 | Assumptions and their implications of the Community Land Model Urban (CLMU) and the integrated Building Energy Model (BEM)

The CLMU models the global urban area with a comprehensive global urban dataset specifically developed for CESM2. It contains present-day urban morphological (e.g., urban extent, building height, street width, pervious ground fraction), thermal (e.g., heat capacity and thermal conductivity), and radiative (e.g., albedo and emissivity) properties, as well as building interior maximum and minimum thermostat settings (cooling and heating setpoint temperatures, respectively) that control the need for H&C. The urban extent is derived from a population density dataset at 1km resolution. The three urban land units correspond to three urban density types (i.e., tall building district, TBD; high density, HD; and medium density, MD) to represent city core, commercial/industrial, and residential areas, the boundaries of which are decided through population density and satellite imagery and vary across regions. Urban building morphological, thermal, and radiative properties are derived from a variety of data sources such as local building codes, municipal documentation, and published construction data and validated against Google Earth imagery[24]. They can be defined uniquely for thirty-three regions of similar physical and social characteristics spanning the global land surface and for each density class (see refs.[22,24] for details).

Given the global scale and the relatively coarse spatial resolution, the goal of the CLMU-BEM is to simulate the average building energy behavior within the constraints of global-scale datasets and computational efficiency. As a result, the BEM includes all key processes that are climate relevant and temperature sensitive, but compromises between the global scale and the computational resources within an ESM as well as data availability on the parameterization of

other processes on a global scale. Solar heat gain through windows due to direct solar radiation is neglected due to a lack of data, but the effects of windows on the overall heat transfer properties of walls are accounted for. The heat storage by internal construction materials and internal heat gains from appliances and occupants are not parameterized in the current version of the CLMU. This implies a possible overestimation of heating and underestimation of cooling energy demand. While these processes are important components of a building's thermal load, they are much less sensitive to ambient temperature, and therefore do not respond much to global warming. Solar heat gain through windows depends on solar radiation, which has been shown to remain relatively constant throughout the 21st century[25]. Internal heat gains through appliances and occupants may experience diurnal variations, weekday/weekend differences, or seasonal differences due to gas usage[26], but they would not be assumed to change over the years unless due to socioeconomic factors (such as replacing the appliances), which is outside the scope of our study. Similarly, internal heat storage from internal construction materials may change over the long term due to building stock changes that are largely socioeconomic driven. As we focus on the changes in H&C energy demand over the century, the effects are likely negligible at the spatiotemporal scale of this study.

We note in Methods that two sources of excess heat from H&C are added as sensible heat to the canyon floor: 1) the heat removed from indoors to outdoors by air conditioning, and 2) the waste heat generated due to inefficiencies, which includes the inefficiencies of the heating and cooling equipment, as well as energy losses in the conversion of primary to end-use energy (such as converting fossil fuel to electricity for cooling). Since CLMU is a single layer urban canopy model, the added sensible heat will dissipate through the urban canyon as the entire urban canopy layer is

represented by a single air temperature. This may lead to shifted and mitigated diurnal profiles, hence not ideal for studying the diurnal variations of the feedback effects. However, such effects are negligible on a monthly timescale used in this study's analysis. This is evidenced by our model's good reproducibility of the two-way feedback effects (see Methods). Our T_u-Q_{AH} sensitivities are also in good agreement with those presented in ref.[27] (Extended Data Table 2). The BEM in CESM2 uses the coefficients of performance (COPs) and weighted efficiencies (p_{eff}) to represent the equipment efficiency of H&C appliances and the conversion efficiency for generating energy used for H&C, respectively. These coefficients are based on the efficiencies of H&C appliances, power plants, and energy mixes from published literature, and readers are directed to refs.[22,28] for further information. Here we note the conversion losses from primary energy in reality may not be necessarily released in areas co-located with the energy from redistributed indoor heat or inefficiencies in the H&C equipment as the model assumes. This could potentially result in some misattributions of feedback effects if the primary energy conversion occurs remotely. To evaluate the sensitivity of this assumption, we conduct two additional land-only simulations: one control (CTRL) run with CLM driven by the atmospheric forcings from a fully-coupled CESM2 CMIP6 SSP5-8.5 simulation and one experiment (NOWSTH) run with identical configuration to the CTRL run except with no waste heat added to the urban canyon. The CTRL run is nearly identical to the CESM2 CMIP6 SSP5-8.5 runs used in this study and also ensures the consistency to compare with the NOWSTH run. The mean absolute differences between NOWSTH and CTRL are 0.006 W/m^2 in Q_C and 0.02 W/m^2 in Q_H across all grid cells over the entire projection period. These differences are two orders of magnitude smaller than the respective mean projected changes of these variables by the model, demonstrating the fidelity of our results.

H&C ownership rates are implicitly modeled by the space heating and cooling setpoints; that is, for places with higher H&C ownership rates, the setpoints are closer to the realistic setpoints we might expect in an individual building, and vice versa. Taking cooling as an example, regions with higher air-conditioning ownership rates have lower cooling setpoints that are closer to what the thermostat settings would be in an actual building. Once the urban air temperature increases to the point that would result in the indoor air temperature going above the setpoint, the infinite-capacity air conditioner removes all excess heat so the indoor air temperature does not exceed the setpoint. After that, the indoor temperature is reset to the setpoint. Having a higher setpoint would mean the air conditioners only work during hotter time periods, which is approximately equivalent to having less air conditioners in an urban area. This explains the large variations in the H&C setpoints employed in the study, and a much higher cooling setpoints in regions with low present-day air-conditioning ownership rates such as the Jakarta region (Supplementary Table 2). The setpoints are part of the urban dataset and can vary across global regions and three urban density types within one grid cell, but are kept constant temporally to isolate climate change effects to achieve the goal of this study.

Supplementary Notes 4 | Training, validating, and applying the urban climate-energy emulators for global multi-model urban projections

The urban climate-energy emulators used in this study are location-specific fully connected neural networks that mimic an urban land model, taking in all atmospheric forcing fields that dynamically drive the urban model in CESM2 and producing specific responses as a result of local urban characteristics and their dynamic interactions with the atmosphere (Extended Data Fig. 7). The atmospheric forcing fields used as inputs to the emulators are monthly average air temperature and humidity, wind speed, precipitation, and downward solar (shortwave) and longwave radiation from the lowest level of the atmosphere model. An indicator variable of the month of year is added to help capture the seasonality. The target variables are monthly average urban 2-meter diurnal mean air temperature (T_u), monthly mean heating (Q_H) and cooling (Q_C) energy demand fluxes.

The training datasets are from three CESM2 CMIP6 ensemble member runs for each of the three scenarios. Each ensemble member is initialized from a slightly perturbed historical simulation and forced by the same climate change forcing specified by the scenario. The resultant projections reflect different realizations of future climates under the same climate change scenario and the internal climate variability[29]. Using more than one ensemble member for training can prevent the emulators from overfitting to one particular climate realization that may not generalize well. From the three ensemble member runs available, two are used for training (for the emulators to learn the parameters) and one for test (to evaluate the performance of the trained emulators).

Before training, the forcing variables are standardized (z-scored) as it is found to provide more stability for training, and the month of year indicator is represented by a 12-dimentional binary vector (i.e., one-hot encoded). Extremely small values ($<10^{-8}$ W m^{-2}) of Q_H and Q_C are set to zero, as they are believed to be either numerical fluctuations or a small transient energy demand being averaged into a monthly value. The Q_H and Q_C values are converted to kJ m^{-2} before training to increase the target values, as it is found to provide better performance.

The emulators share the same architecture, with two dense hidden layers of 8 and 4 units each. They are optimized by an Adam optimizer to minimize the root mean squared error (RMSE). Other hyperparameters (learning rate, batch size, number of epochs, and L1, L2 regularization) are tuned through a 7-fold cross validation using a Bayesian search through the preset hyperparameter space. Because of the high computational cost, 15 grid cells from the U.S. and 15 from the rest of the world are randomly selected to conduct the Bayesian search, and the median of the best hyperparameters were applied to all emulators.

To make multi-model, multi-scenario projections of urban climate and energy, we select 24 models from the Coupled Model Intercomparison Project version 6 (CMIP6). The CMIP6 is a concerted international modeling effort to understand climate variability and change that is used in IPCC Sixth Assessment Report. The Scenario Model Intercomparison Project (ScenarioMIP)[30] is a primary activity within CMIP6 that provides multi-model climate projections based on alternative scenarios of future emissions and land use changes that are directly relevant to societal concerns regarding climate change mitigation, adaptation, or impacts[31]. Among more than 50 models that participated in ScenarioMIP, we selected 20 – 24 models to generate multi-model, multi-scenarios projections based on their resolution (similar or finer resolutions to

CESM2) and data availability (not all ESMs participate in all scenarios). A complete list of models used for each scenario can be found in Supplementary Table 1. To apply the emulators to other ESMs, the atmospheric forcing fields from other ESMs required as input to the emulators are regridded to align with the CESM2 grid (0.9° latitude ×1.25° longitude). This ensures all ESMs have the same set of grid cells where the location-specific emulators are based.

Supplementary Notes 5 | The effect of wind on H&C energy demand.

Urban wind affects building energy demand in two primary ways[32]: (1) through changing the turbulent heat fluxes between the building and the urban environment, and (2) through changing building ventilation and infiltration. For (1), the wind fields directly adjacent to the buildings affect building energy use by changing the convective heat transfer process and urban air temperature. The CLMU calculates urban canopy wind based on a parameterized wind profile and does not resolve turbulence explicitly. This is a recognized and widely adopted approach in local, regional, and global land surface models (both urban and non-urban) to solve urban temperature[33–36]. This approach recognizes the different scale dependence of urban wind and urban temperature. Wind fields within the urban canopy layer (UCL) are turbulence-dominated, and significantly affected by the local roughness of urban surfaces (such as buildings of different heights and shapes, parks, street trees, etc.). Therefore, urban wind fields vary at small scales (on the order of one to ten meters). By contrast, urban temperature and humidity are reasonably well mixed across larger scales (on the order of a few hundred meters to kilometers), which is the scale at which the CLMU operates and simulates urban processes. The parameterization of urban wind profile is an "averaging" of urban wind fields to represent wind at the larger, temperature-relevant scale. It allows CLMU to estimate the average aerodynamic resistance to heat transfer, which then enables the model to accurately simulate urban air temperatures and the average convective heat transfer between the average building and its surrounding environment. Our validation of the two-way temperature-energy sensitivities with 30 country-, regional-, and city-scale case studies (see "Validation of the BEM" in Methods) shows the CLMU-BEM is able to well reproduce their results, which include observations (e.g., refs.[26,37,38]) and simulated results from models that resolve turbulence (e.g., ref.[23]) (Extended Data Tables 1 and 2). This shows that although CLMU

does not resolve the wind fields directly adjacent to the building, the wind effect on building energy use is largely captured in CLMU, and demonstrates the robustness of CLMU in modeling the urban environment and its interaction with building energy use.

For (2), The CLMU-BEM parameterizes ventilation at a fixed rate of 0.3 air-change per hour (ACH). It is not forced mechanically (therefore it does not directly add to the H&C energy demand projected in the study) and does not vary with urban wind. To evaluate the effects of changing ventilation on the H&C demand projections given the constraints of CESM2, we conducted three additional land-only simulations with varying ventilation rates to approximate the potential effects of natural ventilation on H&C energy demand projections. We conduct land-only simulations driven by SSP3-7.0 forcings over the same projection period (2015 – 2099). The run with default ventilation rate (ACH03) is nearly identical with the model results analyzed in the manuscript. The model is also run for no ventilation (ACH00) and an enhanced ventilation at 0.5 ACH (ACH05) as specified by the upper limit in ref.[39].

Compared with no ventilation (ACH00), default ventilation rate (ACH03) results in up to 1 W m^{-2} more cooling energy demand and 2 W m^{-2} more heating energy demand by the end of the century (Supplementary Fig. 4). Southern U.S. and the Middle East show the highest ventilation-induced cooling penalties, whereas the northern U.S., Canada, eastern Europe, colder parts of the Middle East and Asia all experience ventilation induced heating penalties. Parts of Brazil experience a small decrease in cooling energy use due to the benefit of natural ventilation cooling (Supplementary Fig. 4a). This ventilation-induced cooling benefit is more evident when examined on a monthly time scale (Supplementary Fig. 5). Natural ventilation tends to be beneficial in

reducing cooling demand in Spring (March-April-May in the northern hemisphere and September-October-November in the southern hemisphere) when it is not too hot. For Brazil, the cooling benefit is consistent throughout the warmer months. Ventilation increases heating demand in all months when heating is needed (Supplementary Fig. 6). Similar trends of smaller magnitude can be observed when we compare the high ventilation rate run (ACH05) with the default ventilation rate run (ACH03), hence not shown.

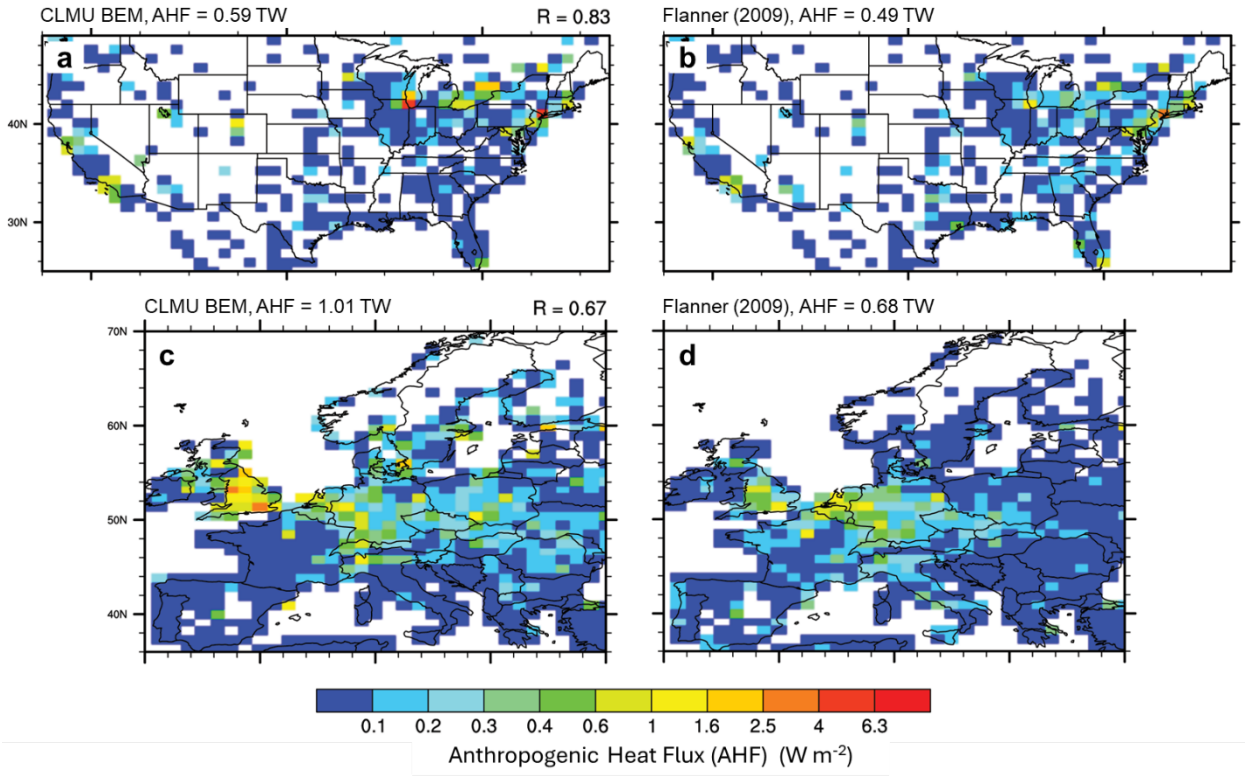

Supplementary Fig. 1 | Comparison of anthropogenic heat flux (AHF) due to H&C over the U.S. (a, b) and Europe (c, d) from the (a, c) CLMU-BEM modeled results and (b, d) Flanner observation-based dataset[40]. The observational total AHF from all sources has been multiplied by 16% (**b**) and 25% (**d**) to adjust it for energy due only to space heating and cooling in the U.S. and Europe, respectively, based on estimates for the proportions of H&C energy use in total energy consumption (see ref.[22] for more details). The modeled and the observational data have been masked for each other's urban areas. R is the pattern correlation between the model simulations and observations. Basemap information is available in NCAR Command Language Manual (https://www.ncl.ucar.edu/Document/Graphics/Resources/mp.shtml).

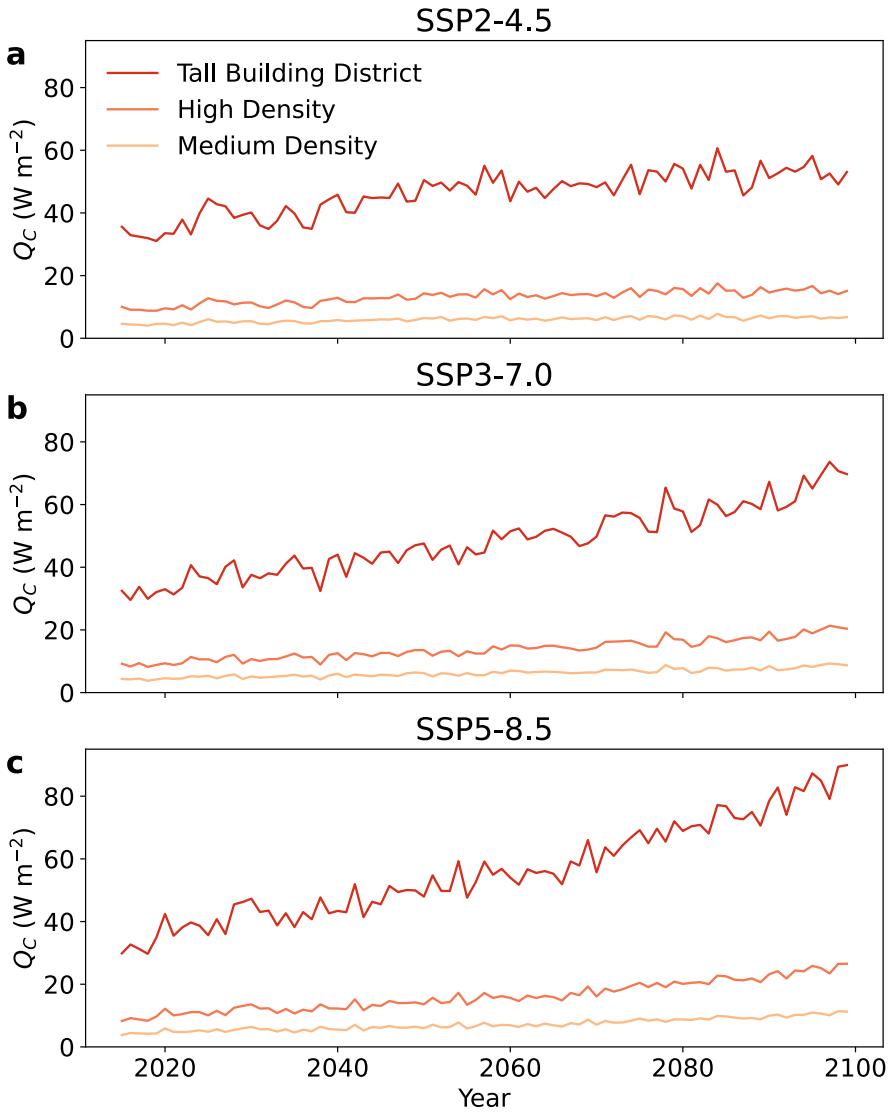

Supplementary Fig. 2 | Higher urban density leads to faster and larger increase in cooling energy demand in Miami. a-c, time series of annual mean Q_C for three urban density types (tall building district, high density, and medium density) under SSP2-4.5 (**a**), SSP3-7.0 (**b**), and SSP5-8.5 (**c**) in the grid cell that contains Miami, Florida, USA. It contains all three urban density types and has near saturated and equal air-conditioning ownership rate across the three density types (Supplementary Table 2). Because multi-model projections are only made for the area-weighted average of the whole urban area, only CESM2 result is plotted.

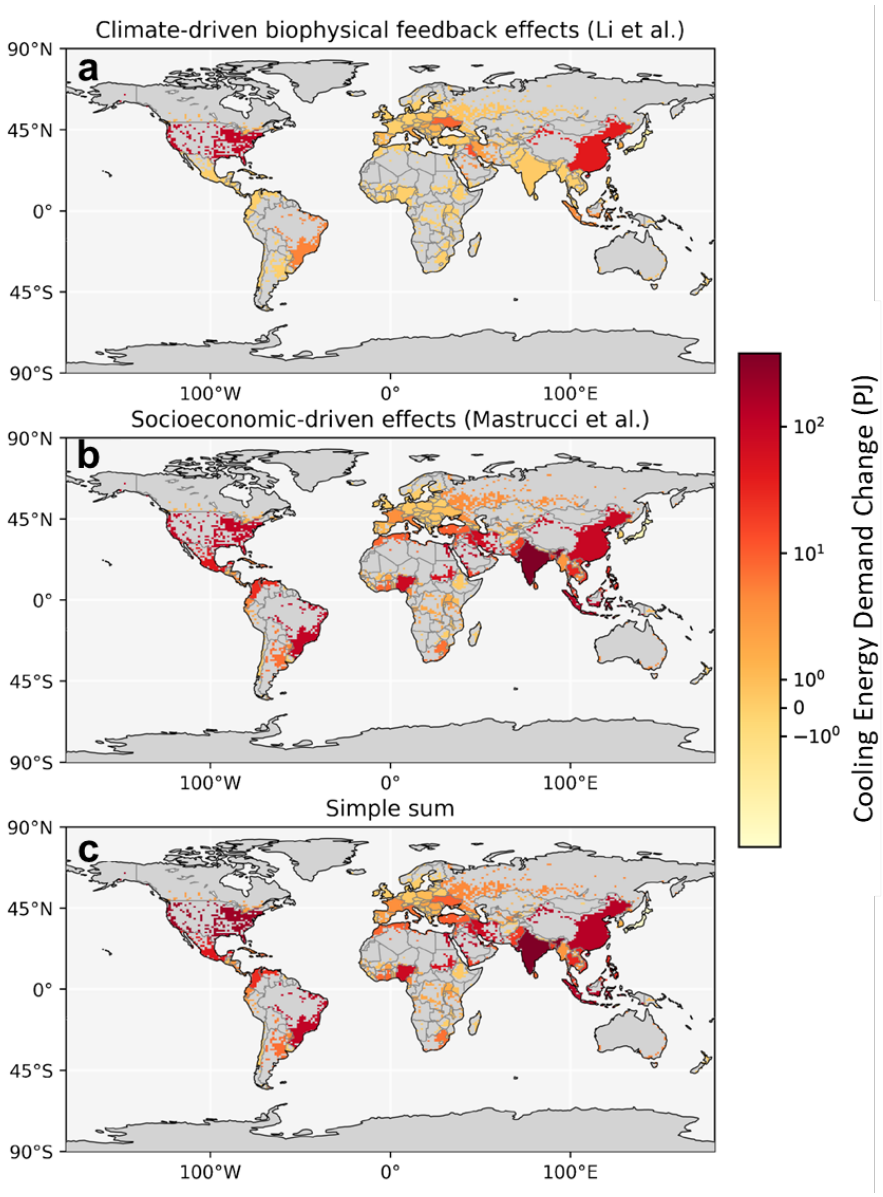

Supplementary Fig. 3 | Climate-driven increase in cooling energy demand is comparable in magnitude with purely socioeconomic-driven increase. Changes in urban cooling energy demand (in PJ) between 2015 and 2050 under SSP3-7.0 driven by (**a**) climate change only (this study) and (**b**) socioeconomic development only (ref.[17]). A simple sum is presented in **c** as a first-order approximation and a lower bound of the combined effects. Basemap from Natural Earth (https://www.naturalearthdata.com/).

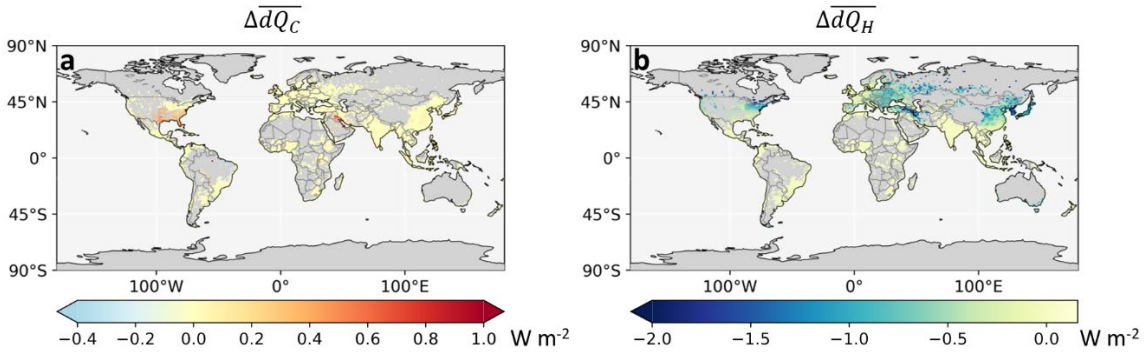

Supplementary Fig. 4 | Increased ventilation induces small cooling and heating energy penalty for most places. a and **b,** changes in decadal average (last decade, 2090 – 2099, minus first decade, 2015 – 2024, represented by Δ) of the difference between default ventilation rate (ACH03) and no ventilation (ACH00) runs (represented by *d*) for cooling (**a**) and heating (**b**) energy demand, under SSP3-7.0. Basemap from Natural Earth (https://www.naturalearthdata.com/).

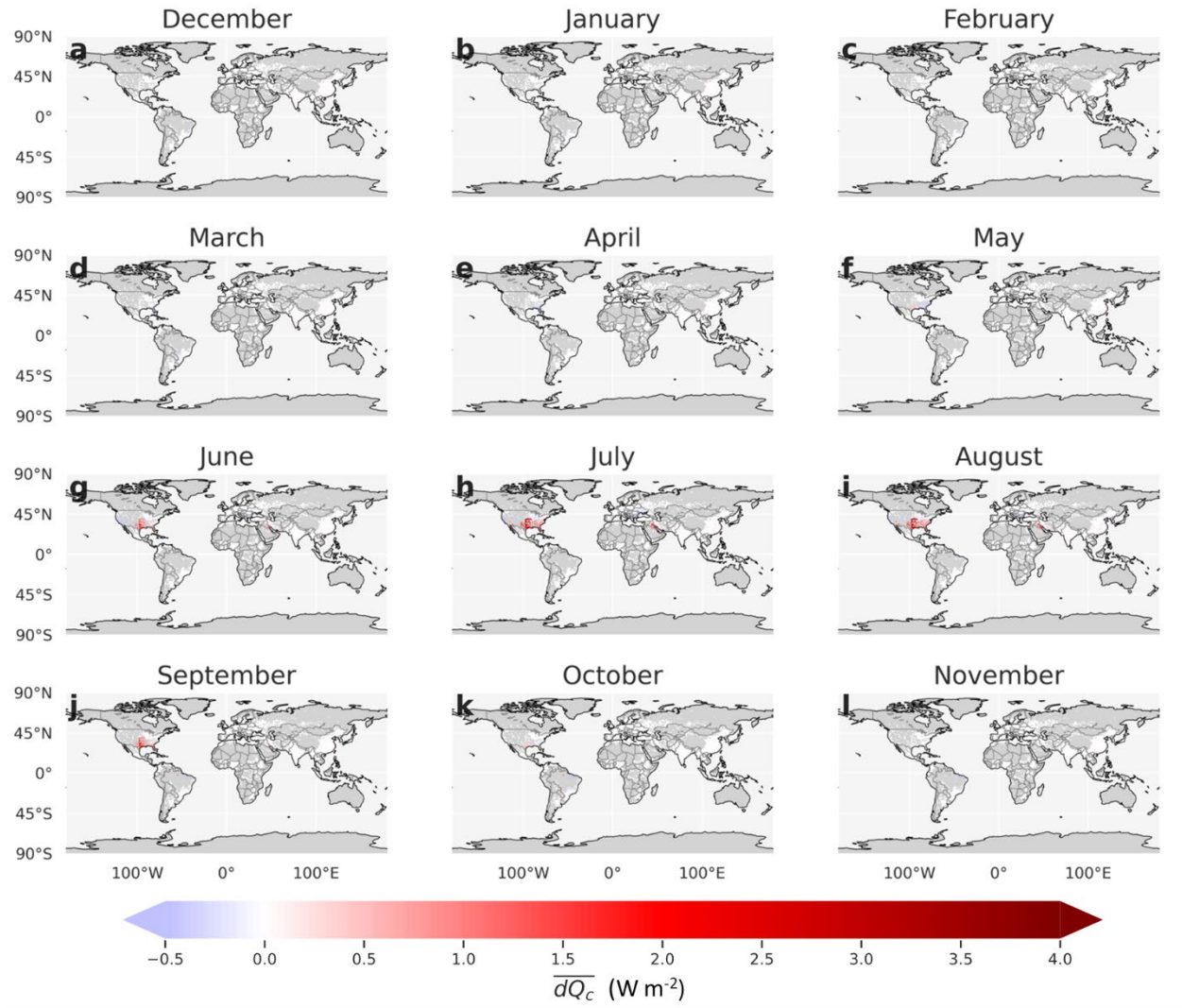

Supplementary Fig. 5 | Natural ventilation is beneficial in reducing cooling demand in Spring. a – **l**, average difference in monthly mean cooling energy demand flux for the 12 months between default ventilation (ACH03) and no ventilation (ACH00) runs for 2015 – 2099 under SSP3-7.0. Basemap from Natural Earth (https://www.naturalearthdata.com/).

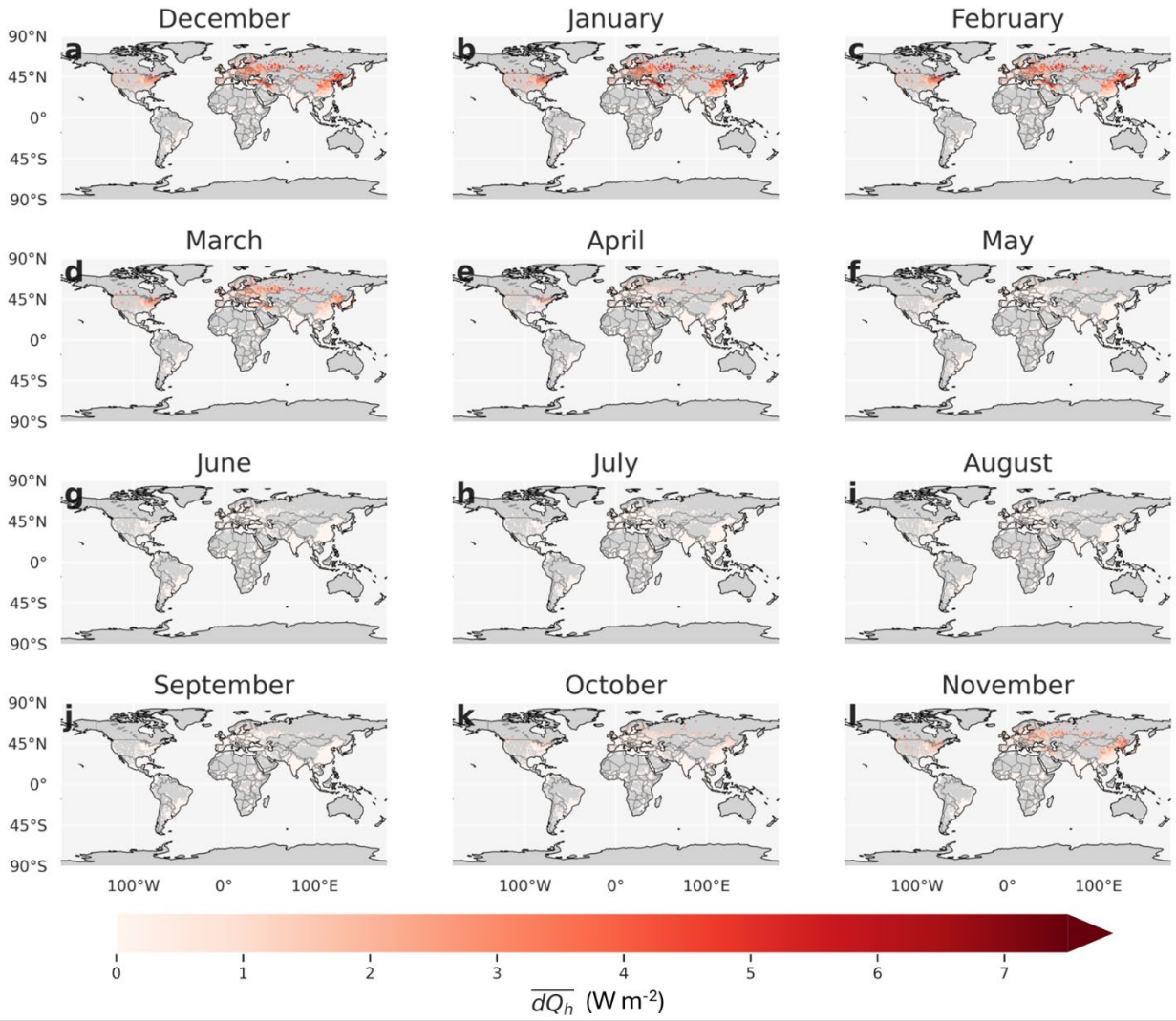

Supplementary Fig. 6 | Natural ventilation leads to increased heating energy demand. a – l, average difference in monthly mean heating energy demand flux for the 12 months between default ventilation (ACH03) and no ventilation (ACH00) runs for 2015 – 2099 under SSP3-7.0. Basemap from Natural Earth (https://www.naturalearthdata.com/).

Supplementary Table 1 | List of CMIP6 ESMs analyzed in this study (including CESM2) under each scenario.

	Model name	Spatial resolution (latitude × longitude)	SSP2-4.5	SSP3-7.0	SSP5-8.5
1	ACCESS-CM2	1.25° × 1.875°	✓	✓	✓
2	ACCESS-ESM1-5	1.25° × 1.875°	✓	✓	✓
3	AWI-CM-1-1-MR	0.94° × 0.94°	✓	✓	✓
4	BCC-CSM2-MR	1.125° × 1.125°	✓	✓	✓
5	CESM2	0.9° × 1.25°	✓	✓	✓
6	CMCC-CM2-SR5	1° × 1°	✓	✓	✓
7	CNRM-CM6-1-HR	0.5° × 0.5°	✓	✓	✓
8	CNRM-ESM2-1	1.41° × 1.41°		✓	✓
9	EC-Earth3	0.7° × 0.7°	✓	✓	✓
10	EC-Earth3-Veg	0.7° × 0.7°	✓	✓	✓
11	FGOALS-f3-L	1° × 1°	✓	✓	✓
12	FIO-ESM-2-0	0.9° × 1.25°	✓		✓
13	GFDL-CM4	1° × 1°	✓		✓
14	GFDL-ESM4	1° × 1°	✓	✓	✓
15	GISS-E2-1-G	2° × 2.5°	✓	✓	✓
16	HadGEM3-GC31-MM	0.55° × 0.83°			✓
17	INM-CM4-8	1.5° × 2°	✓	✓	✓
18	INM-CM5-0	1.5° × 2°	✓	✓	✓
19	IPSL-CM6A-LR	1.27° × 2.5°	✓	✓	✓
20	KACE-1-0-G	1.25° × 1.875°	✓	✓	✓
21	MIROC6	1.39° × 1.41°	✓	✓	✓
22	MPI-ESM1-2-HR	0.92° × 0.94°	✓	✓	✓
23	MRI-ESM2-0	1.11° × 1.125°	✓	✓	✓
24	NESM3	1.875° × 1.875°	✓		✓
25	NorESM2-MM	0.9° × 1.25°	✓	✓	✓

Supplementary Table 2 | Key model parameterizations and climates for selected cities in Fig. 5 and Extended Data Fig. 4. *H/W* is the building height to street width ratio, W_{roof} is the roof fraction, and f_{prvrd} is the pervious fraction of canyon floor (all unitless). The values are provided for each urban density types: tall building district (TBD), high density (HD) and medium density (MD). Roof and wall materials are used to derive values for thermal conductivity and heat capacity as described in ref.[24]. Space cooling (heating) is controlled by cooling (heating) setpoints and are proxies for H&C ownership (see Supplementary Notes 3). "-" indicates absence of the urban density type.

City	**Köppen climate classification**	***H/W*** (TBD, HD, MD)	W_{roof} (TBD, HD, MD)	f_{prvrd} (TBD, HD, MD)	**Roof materials***	**Wall materials***	**Cooling setpoints (°C)** (TBD, HD, MD)	**Heating setpoints (°C)** (TBD, HD, MD)
Athens, Greek	Csa	-, 1.8, 0.75	-, 0.55 0.40	-, 0.33, 0.58	Ceramic tiles/wood deck, built-up roof concrete deck, galvanized steel	Brick and concrete masonry	32, 37, 37	17, 17, 12
Los Angeles, California, USA	Csb	5.2, 1.6, 0.48	0.6, 0.6, 0.55	0.13, 0.25, 0.56	Built-up roof concrete deck, insulated steel deck, galvanized steel, ceramic tiles/wood deck	Concrete panels & masonry, glass curtain, brick, wood frame with insulated façade	27, 32, 32	19, 17, 17
Jakarta, Indonesia	Af	3.6, 1.2, 0.67	0.55, 0.6, 0.35	0.33, 0.38, 0.92	Ceramic tiles/wood deck, built-up roof wood deck, Built-up roof concrete deck, galvanized steel	Concrete panels & masonry, glass curtain, stone curtain, concrete blocks	32, OFF, OFF	17, 12, 5
Miami, Florida, USA	Aw	4, 1.6, 0.48	0.65, 0.55, 0.55	0.14, 0.33, 0.67	Built-up roof concrete deck, galvanized steel, Shingles/wood deck, metal tiles	Concrete panels & masonry, glass curtain, brick, wood frame with insulated façade, stone curtain	27, 27, 27	19, 17, 17
Tehran, Iran	Csa	8, 1.8, 0.8	0.5, 0.8, 0.65	0.20, 0.25, 0.43	Built-up roof concrete deck, insulated steel deck, ceramic tiles/wood deck	Concrete panels & masonry, glass curtain, brick (reinforced), concrete blocks	32, 42, OFF	17, 12, 5
Riyadh, Saudi Arabia	BWh	8, 1.8, 0.8	0.5, 0.8, 0.65	0.20, 0.25, 0.43	Built-up roof concrete deck, insulated steel deck, ceramic tiles/wood deck	Concrete panels & masonry, glass curtain, brick (reinforced), concrete blocks	32, 42, OFF	17, 12, 5

Hong Kong, China	Cfa	7.2, 1.8, 0.48	0.5, 0.6, 0.35	0.20, 0.38, 0.62	Built-up roof concrete deck, insulated steel deck, galvanized steel, built-up roof wood deck, ceramic tiles/wood deck	Concrete panels & masonry, glass curtain, brick, brick (reinforced)	27, 37, 37	19, 12, 12
Chongqing, China	Cfa	7.2, 1.8, 0.48	0.5, 0.6, 0.35	0.20, 0.38, 0.62	Built-up roof concrete deck, insulated steel deck, galvanized steel, built-up roof wood deck, ceramic tiles/wood deck	Concrete panels & masonry, glass curtain, brick, brick (reinforced)	27, 37, 37	19, 12, 12

*These are the main materials that make up the building façades in each urban density type.

Some materials are shared across density types.

References

1. Salamanca, F., Georgescu, M., Mahalov, A., Moustaoui, M. & Wang, M. Anthropogenic heating of the urban environment due to air conditioning. *Journal of Geophysical Research: Atmospheres* **119**, 5949–5965 (2014).
2. Takane, Y., Kikegawa, Y., Hara, M. & Grimmond, C. S. B. Urban warming and future air-conditioning use in an Asian megacity: importance of positive feedback. *npj Climate and Atmospheric Science* **2**, 1–11 (2019).
3. Hsieh, C.-M., Aramaki, T. & Hanaki, K. The feedback of heat rejection to air conditioning load during the nighttime in subtropical climate. *Energy and Buildings* **39**, 1175–1182 (2007).
4. Kikegawa, Y., Nakajima, K., Takane, Y., Ohashi, Y. & Ihara, T. A quantification of classic but unquantified positive feedback effects in the urban-building-energy-climate system. *Applied Energy* **307**, 118227 (2022).
5. Pokhrel, R., Ortiz, L. E., Ramírez-Beltran, N. D. & González, J. E. On the Climate Variability and Energy Demands for Indoor Human Comfort Levels in a Tropical-Coastal Urban Environment. *Journal of Solar Energy Engineering* **141**, (2018).
6. Ortiz, L., González, J. E. & Lin, W. Climate change impacts on peak building cooling energy demand in a coastal megacity. *Environ. Res. Lett.* **13**, 094008 (2018).
7. Kheiri, F., Haberl, J. S. & Baltazar, J.-C. Impact of outdoor humidity conditions on building energy performance and environmental footprint in the degree days-based climate classification. *Energy* **283**, 128447 (2023).
8. Guan, H., Beecham, S., Xu, H. & Ingleton, G. Incorporating residual temperature and specific humidity in predicting weather-dependent warm-season electricity consumption. *Environ. Res. Lett.* **12**, 024021 (2017).

9. Rastogi, D. *et al.* The role of humidity in determining future electricity demand in the southeastern United States. *Environ. Res. Lett.* **16**, 114017 (2021).
10. van Ruijven, B. J., De Cian, E. & Sue Wing, I. Amplification of future energy demand growth due to climate change. *Nat Commun* **10**, 2762 (2019).
11. Hadley, S. W., Erickson III, D. J., Hernandez, J. L., Broniak, C. T. & Blasing, T. J. Responses of energy use to climate change: A climate modeling study. *Geophysical Research Letters* **33**, (2006).
12. Isaac, M. & van Vuuren, D. P. Modeling global residential sector energy demand for heating and air conditioning in the context of climate change. *Energy Policy* **37**, 507–521 (2009).
13. Auffhammer, M., Baylis, P. & Hausman, C. H. Climate change is projected to have severe impacts on the frequency and intensity of peak electricity demand across the United States. *PNAS* **114**, 1886–1891 (2017).
14. Levesque, A. *et al.* How much energy will buildings consume in 2100? A global perspective within a scenario framework. *Energy* **148**, 514–527 (2018).
15. Salamanca, F., Georgescu, M., Mahalov, A. & Moustaoui, M. Summertime Response of Temperature and Cooling Energy Demand to Urban Expansion in a Semiarid Environment. *Journal of Applied Meteorology and Climatology* **54**, 1756–1772 (2015).
16. Perera, A. T. D., Javanroodi, K. & Nik, V. M. Climate resilient interconnected infrastructure: Co-optimization of energy systems and urban morphology. *Applied Energy* **285**, 116430 (2021).
17. Mastrucci, A., van Ruijven, B., Byers, E., Poblete-Cazenave, M. & Pachauri, S. Global scenarios of residential heating and cooling energy demand and CO2 emissions. *Climatic Change* **168**, 14 (2021).

18. Pokhrel, R., Walker, A. & González, J. E. A New Methodology to Assess Building Integrated Roof Top Photovoltaic Installations at City Scales: The Tropical Coastal City Case. *ASME Journal of Engineering for Sustainable Buildings and Cities* **1**, (2019).
19. Ortiz, L. E., Gonzalez, J. E., Gutierrez, E. & Arend, M. Forecasting Building Energy Demands With a Coupled Weather-Building Energy Model in a Dense Urban Environment. *Journal of Solar Energy Engineering* **139**, (2016).
20. Salamanca, F., Georgescu, M., Mahalov, A., Moustaoui, M. & Martilli, A. Citywide Impacts of Cool Roof and Rooftop Solar Photovoltaic Deployment on Near-Surface Air Temperature and Cooling Energy Demand. *Boundary-Layer Meteorol* **161**, 203–221 (2016).
21. Gutiérrez, E., González, J. E., Martilli, A. & Bornstein, R. On the Anthropogenic Heat Fluxes Using an Air Conditioning Evaporative Cooling Parameterization for Mesoscale Urban Canopy Models. *Journal of Solar Energy Engineering* **137**, (2015).
22. Oleson, K. W. & Feddema, J. Parameterization and Surface Data Improvements and New Capabilities for the Community Land Model Urban (CLMU). *Journal of Advances in Modeling Earth Systems* e2018MS001586 (2020) doi:10.1029/2018MS001586@10.1002/(ISSN)1942-2466.CESM2.
23. Gamarro, H. & González-Cruz, J. E. On the Electrification of Winter Season in Cold Climate Megacities—The Case of New York City. *ASME Journal of Engineering for Sustainable Buildings and Cities* **4**, (2023).
24. Jackson, T. L., Feddema, J. J., Oleson, K. W., Bonan, G. B. & Bauer, J. T. Parameterization of Urban Characteristics for Global Climate Modeling. *Annals of the Association of American Geographers* **100**, 848–865 (2010).

25. Li, D. H. W., Yang, L. & Lam, J. C. Impact of climate change on energy use in the built environment in different climate zones – A review. *Energy* **42**, 103–112 (2012).
26. Nakajima, K., Takane, Y., Kikegawa, Y. & Yamaguchi, K. Improvement of WRF–CM–BEM and its application to high-resolution hindcasting of summertime urban electricity consumption. *Energy and Buildings* **296**, 113336 (2023).
27. Wang, L., Sun, T., Zhou, W., Liu, M. & Li, D. Deciphering the sensitivity of urban canopy air temperature to anthropogenic heat flux with a forcing-feedback framework. *Environ. Res. Lett.* **18**, 094005 (2023).
28. Sivak, M. Air conditioning versus heating: climate control is more energy demanding in Minneapolis than in Miami. *Environ. Res. Lett.* **8**, 014050 (2013).
29. Rodgers, K. B. *et al.* Ubiquity of human-induced changes in climate variability. *Earth System Dynamics* **12**, 1393–1411 (2021).
30. O'Neill, B. C. *et al.* The Scenario Model Intercomparison Project (ScenarioMIP) for CMIP6. *Geoscientific Model Development* **9**, 3461–3482 (2016).
31. Tebaldi, C. *et al.* Climate model projections from the Scenario Model Intercomparison Project (ScenarioMIP) of CMIP6. *Earth System Dynamics* **12**, 253–293 (2021).
32. Jie, P. *et al.* Impact of urban wind environment on urban building energy: A review of mechanisms and modeling. *Building and Environment* **245**, 110947 (2023).
33. Masson, V. A Physically-Based Scheme For The Urban Energy Budget In Atmospheric Models. *Boundary-Layer Meteorology* **94**, 357–397 (2000).
34. Järvi, L., Grimmond, C. S. B. & Christen, A. The Surface Urban Energy and Water Balance Scheme (SUEWS): Evaluation in Los Angeles and Vancouver. *Journal of Hydrology* **411**, 219–237 (2011).

35. Kusaka, H., Kondo, H., Kikegawa, Y. & Kimura, F. A Simple Single-Layer Urban Canopy Model For Atmospheric Models: Comparison With Multi-Layer And Slab Models. *Boundary-Layer Meteorology* **101**, 329–358 (2001).
36. Lawrence, D. *et al.* Technical Description of version 5.0 of the Community Land Model (CLM). (2020).
37. Kikegawa, Y., Tanaka, A., Ohashi, Y., Ihara, T. & Shigeta, Y. Observed and simulated sensitivities of summertime urban surface air temperatures to anthropogenic heat in downtown areas of two Japanese Major Cities, Tokyo and Osaka. *Theor Appl Climatol* **117**, 175–193 (2014).
38. Chen, M., Ban-Weiss, G. A. & Sanders, K. T. Utilizing smart-meter data to project impacts of urban warming on residential electricity use for vulnerable populations in Southern California. *Environmental Research Letters* **15**, (2020).
39. Sailor, D. J. A review of methods for estimating anthropogenic heat and moisture emissions in the urban environment. *International Journal of Climatology* **31**, 189–199 (2011).
40. Flanner, M. G. Integrating anthropogenic heat flux with global climate models. *Geophysical Research Letters* **36**, (2009).